Photodissociation dynamics of H_2O at 111.5 nm by a vacuum ultraviolet free electron laser

Heilong Wang, Yong Yu, Yao Chang, Shu Su, Shengrui Yu, Qinming Li, Kai Tao, Hongli Ding, Jaiyue Yang, Guanglei Wang, Li Che, Zhigang He, Zhichao Chen, Xingan Wang, Weiqing Zhang, Dongxu Dai, Guorong Wu, Kaijun Yuan, and Xueming Yang

Citation: J. Chem. Phys. **148**, 124301 (2018); doi: 10.1063/1.5022108

View online: https://doi.org/10.1063/1.5022108

View Table of Contents: http://aip.scitation.org/toc/jcp/148/12

Published by the American Institute of Physics

THE JOURNAL OF CHEMICAL PHYSICS 148, 124301 (2018)

Photodissociation dynamics of H_2O at 111.5 nm by a vacuum ultraviolet free electron laser

Heilong Wang,[1,2,a)] Yong Yu,[2,a)] Yao Chang,[2,3] Shu Su,[2] Shengrui Yu,[4] Qinming Li,[2] Kai Tao,[2] Hongli Ding,[2] Jaiyue Yang,[2] Guanglei Wang,[2] Li Che,[1,5,b)] Zhigang He,[2] Zhichao Chen,[2] Xingan Wang,[3,b)] Weiqing Zhang,[2] Dongxu Dai,[2] Guorong Wu,[2] Kaijun Yuan,[2,b)] and Xueming Yang[2,b)]

[1]*College of Environmental Sciences and Engineering, Dalian Maritime University, 1 Linghai Road, Dalian, Liaoning 116026, People's Republic of China*

[2]*State Key Laboratory of Molecular Reaction Dynamics, Dalian Institute of Chemical Physics, 457 Zhongshan Road, Dalian, Liaoning 116023, People's Republic of China*

[3]*Center for Advanced Chemical Physics (iChEM, Collaborative Innovation Center of Chemistry for Energy Materials), Department of Chemical Physics, School of Chemistry and Materials Science, University of Science and Technology of China, Jinzhai Road 96, Hefei, Anhui 230026, People's Republic of China*

[4]*Hangzhou Institute of Advanced Studies, Zhejiang Normal University, 1108 Gengwen Road, Hangzhou, Zhejiang 311231, People's Republic of China*

[5]*College of Science, Dalian Maritime University, 1 Linghai Road, Dalian, Liaoning 116026, People's Republic of China*

(Received 11 January 2018; accepted 2 March 2018; published online 22 March 2018)

Photodissociation dynamics of H_2O via the $\tilde{F}$ state at 111.5 nm were investigated using the high resolution H-atom Rydberg "tagging" time-of-flight (TOF) technique, in combination with the tunable vacuum ultraviolet free electron laser at the Dalian Coherent Light Source. The product translational energy distributions and angular distributions in both parallel and perpendicular directions were derived from the recorded TOF spectra. Based on these distributions, the quantum state distributions and angular anisotropy parameters of OH (X) and OH (A) products have been determined. For the OH (A) + H channel, highly rotationally excited OH (A) products have been observed. These products are ascribed to a fast direct dissociation on the $\tilde{B}^1A_1$ state surface after multi-step internal conversions from the initial excited $\tilde{F}$ state to the $\tilde{B}$ state. While for the OH (X) + H channel, very highly rotationally excited OH (X) products with moderate vibrational excitation are revealed and attributed to the dissociation via a nonadiabatic pathway through the well-known two conical intersections between the $\tilde{B}$-state and the $\tilde{X}$-state surfaces. *Published by AIP Publishing.* https://doi.org/10.1063/1.5022108

I. INTRODUCTION

Since its great importance in atmospheric and interstellar chemistry,[1,2] photodissociation of the water molecule in the vacuum ultraviolet (VUV) region has been a fascinating topic in photochemistry. With the development of various experimental techniques and the quantum dynamical calculation methods, the photodissociation dynamics of water have been studied extensively over the past few decades.[3–22] The water molecule in its ground state ($\tilde{X}\,^1A_1$) has C_{2v} symmetry, and the electronic configuration is $(1a_1)^2(2a_1)^2(3a_1)^2(1b_1)^2$. It has rich electronic absorption bands in the VUV region below 200 nm induced by the excitation of one electron from $1b_1$ or $3a_1$ orbital to a Rydberg orbital. The absorption spectra of H_2O in the wavelength region of 190–120 nm consist of two broad, well-separated bands with their maxima at ~167 nm and ~128 nm, respectively.[23] The first absorption band near 190–150 nm is ascribed as the electronic transition $\tilde{A}^1B_1 \leftarrow \tilde{X}^1A_1$ ($3sa_1 \leftarrow 1b_1$). Then, the absorption band around 150–120 nm corresponds to the electronic transition $\tilde{B}^1A_1 \leftarrow \tilde{X}^1A_1$ ($3sa_1 \leftarrow 3a_1$). Superimposed on this continuum is a progression of very diffuse bands with almost constant spacing of about 800 cm^{-1}.[24] Besides, the absorption bands peaked at 124 nm and 122 nm are attributed to the Rydberg transitions, $\tilde{C}^1B_1 \leftarrow \tilde{X}^1A_1$ ($3pa_1 \leftarrow 1b_1$) and $\tilde{D}^1A_1 \leftarrow \tilde{X}^1A_1$ ($3pa_2 \leftarrow 1b_1$), respectively.[25]

Dissociation of H_2O molecules on the $\tilde{A}$ state provides an ideal model of direct dissociation, due to the repulsive potential energy surface along the O–H band, and yields a H atom and a ground state OH with little internal excitation.[6,18,26–31] By contrast, much more complicated and plentiful dynamical information has been concluded from the dissociation of H_2O molecules on the $\tilde{B}$ state, a classical multichannel dissociation process. Three electronic excited states have been involved, i.e., $\tilde{X}$, $\tilde{A}$, and $\tilde{B}$ states. At the linear geometries of H-O-H and O-H-H, two completive conical intersections exist between the $\tilde{B}$ state and the $\tilde{X}$ state, and the Renner-Teller coupling between the $\tilde{B}$ state and the $\tilde{A}$ state is also possible since the energy degeneracy with these geometries.[11,13,32–34] As a result, the initial excitation of H_2O molecules to the $\tilde{B}$ state leads to a direct dissociation process on the $\tilde{B}$ state surface to produce a H atom and an excited electronic state OH

[a)] H. Wang and Y. Yu contributed equally to this work.

[b)] Authors to whom correspondence should be addressed: kjyuan@dicp.ac.cn; xawang@ustc.edu.cn; lichedmu@163.com; and xmyang@dicp.ac.cn fragment through the adiabatic pathway or yields a H atom plus a ground state OH partner through the nonadiabatic pathway from the $\tilde{B}$ state to the potential energy surfaces of either the $\tilde{A}$ state or the ground state $\tilde{X}$ of water. Besides, the three-body dissociation of O (^{1}D, ^{3}P) + 2H is also energetically accessible. The characterization of internal distribution of the OH products is highly vibration-rotation reversal, i.e., rotationally hot but vibrationally cold, which has been revealed from the correlative studies previously.[35–39] More interesting, the striking even-odd intensity oscillations in the ground state OH (X, v = 0) product rotational distribution, which are assigned to the dynamical interference between the two completive conical intersection pathways, have been observed by Harich and co-workers.[38]

The $\tilde{C}^1B_1$ state of H_2O molecules, reached at around 124 nm, is the first Rydberg state with fully resolved rotational structures by one-photon or multi-photon absorptions, due to two essential factors: (1) the $\tilde{C}^1B_1$ Rydberg state is a long-lived (about a few ps) and typical bound state, (2) H_2O molecule has a sufficiently large rotational constant.[40–43] Two different dissociation mechanisms, which are highly dependent with the rotational constant $K_a{}'$, have been revealed from a one-photon induced predissociation dynamics study.[45] It is concluded that, for H_2O in the rotational state with $K_a{}' = 0$, the photodissociation process occurs exclusively via the homogeneous nonadiabatic coupling to the $\tilde{A}^1B_1$ state, leading to rotationally cold and vibrationally hot OH (X) products (up to v = 13, peaked at v = 7). While for H_2O in the rotationally excited state with $K_a{}' > 0$, an additional heterogeneous pathway opens through the Coriolis-type coupling to the $\tilde{B}^1A_1$ state, results in rotationally hot and vibrationally cold ground state OH (X) and electronically excited OH (A) products.[44–46] In addition, the predissociation dynamics of H_2O molecules on the vibrationally excited $\tilde{C}$ state were studied using the time-resolved photoelectron imaging method by Wu *et al.*,[47] and a new predissociation pathway has been observed. Due to the energy degeneracy between the $\tilde{C}$(010) and $\tilde{D}$(000) vibronic states, the initial excited $\tilde{C}$(010) state of H_2O molecules could undergo an accidental resonance predissociated pathway through the $\tilde{D}$(000) state, followed by a strong internal conversion to the $\tilde{B}$ state at a bent geometry.[47]

The dissociation dynamics of H_2O molecules on the $\tilde{D}$ state have also been investigated. Typically, the initial excited $\tilde{D}$ state of H_2O molecules undergoes a fast predissociation process (13.5–50 fs) via an avoided crossing at the bent geometry to the $\tilde{B}$ state, followed by a similar dissociation dynamics with the direct excitation to the $\tilde{B}$ state.[48,49]

Over the past decades, the photodissociation dynamics of H_2O molecules on the initial excited $\tilde{A}$, $\tilde{B}$, $\tilde{C}$, and $\tilde{D}$ states have been studied comprehensively, and the relative quantitative pictures are obtained. Whereas, the study of photodissociation dynamics of H_2O molecules on the higher-lying Rydberg states, like $\tilde{E}$ and $\tilde{F}$ states, is limited, due to the lack of the tunable and intense VUV radiation source. Recently, a new generation tunable VUV free electron laser (FEL) has been built successfully in Dalian [Dalian Coherent Light Source (DCLS)], China, which works mainly in 50–150 nm. In this work, we use the VUV FEL combined with the high resolution H atom Rydberg "tagging" time-of-flight (HRTOF) technique for the first time, to study the photodissociation dynamics of H_2O molecules at 111.5 nm, which excites H_2O molecules to the $\tilde{F}$ state.[15] Product translational energy distributions and angular distributions have been determined. Besides, the internal state distributions as well as the angular anisotropy parameters are also presented in this study.

II. EXPERIMENTAL DETAILS

The experiments are performed in a newly constructed end-station for molecular photochemistry around the VUV-FEL beam line[50] at DCLS. Briefly, The VUV-FEL facility operates in the HGHG (High Gain Harmonic Generation) mode,[51] in which the seed laser is injected to interact with the electron beam in the modulator. The seeding pulse at 240-360 nm is generated by a Ti:sapphire laser. The electron beam produced by a photocathode RF gun is accelerated to the beam energy of ∼300 MeV with a bunch charge of 500 pC. The micro-bunched beam is then sent through the radiator, which is tuned to the nth harmonic of the seed wavelength. As a result, the coherent FEL pulse at λ/n is emitted. The VUV-FEL beam pulse operates at 20 Hz with the pulse energy of >200 μJ/pulse. The wavelength is continuously tunable between 50 and 150 nm, and the typical frequency bandwidth is around ∼50 cm^{-1}.

The HRTOF technique utilized in this study has been described in detail elsewhere.[52,53] In brief, in this study, the molecular beam of H_2O is generated by bubbling Ar through the Ar/H_2O mixture and expanding through a 1.0 mm diameter pulsed nozzle at a stagnation pressure of ∼1 atm. Great efforts have been made on the optimization of the performance of the pulsed valve to minimize the formation of H_2O sample clusters. The rotational temperature of the water molecules in the molecular beam is about 10 K. The molecular beam is then crossed perpendicularly with the photolysis and probe laser light. The polarization of the photolysis VUV-FEL light is horizontal. The H atom products from H_2O photodissociation in the photolysis region are excited from the ground state to a high-n Rydberg state via a two-step excitation scheme: the coherent VUV excitation at the Lyman-α wavelength (121.6 nm) followed by UV photon excitation at about 365 nm. The 121.6 nm VUV light is generated by the difference four-wave mixing method of two 212.5 nm photons and one 845 nm photon in a Kr/Ar (ratio 1:3) mixture gas cell.[54] The 212.5 nm laser light is produced by doubling the output of a tunable dye laser operating at about 425 nm, pumped by the third harmonic output of a Nd:YAG laser, while the 845 nm laser light is the direct output of another dye laser pumped by part of the second harmonic output from the same Nd:YAG laser. The 365 nm laser light is generated by doubling the output of a tunable dye laser operating at about 730 nm, pumped by another part of the second harmonic of the Nd:YAG laser. The photolysis light, 111.5 nm, is generated by FEL. The three excitation laser light beams (212.5, 845, and 365 nm) are overlapped both in space and time in the photolysis region, while the photolysis light beam is crossed with an angle of 7° relative to the 365 nm light in the center of photolysis region.

The charged species at the tagging region generated by the laser beams are extracted away by a small electric field

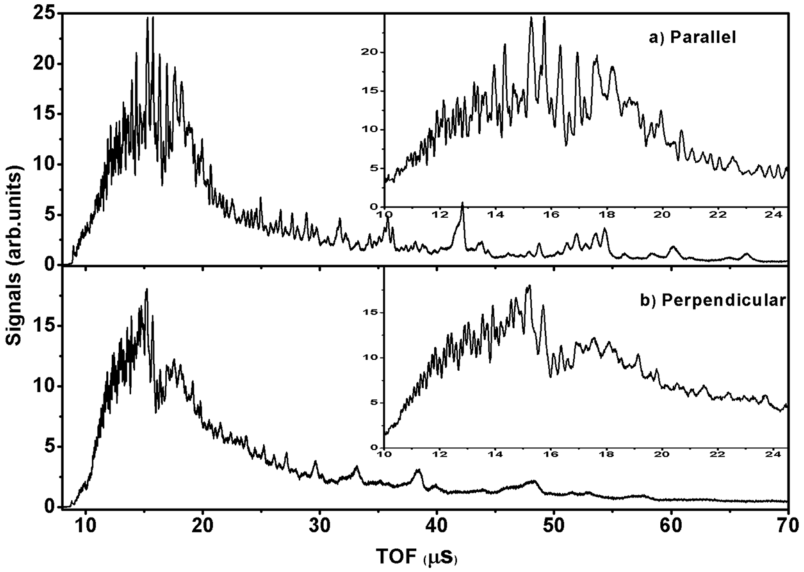

FIG. 1. Time-of-flight spectra of the H atom product from the photodissociation of H_2O at 111.5 nm with the detection axis parallel (a) and perpendicular (b) to photolysis laser polarization.

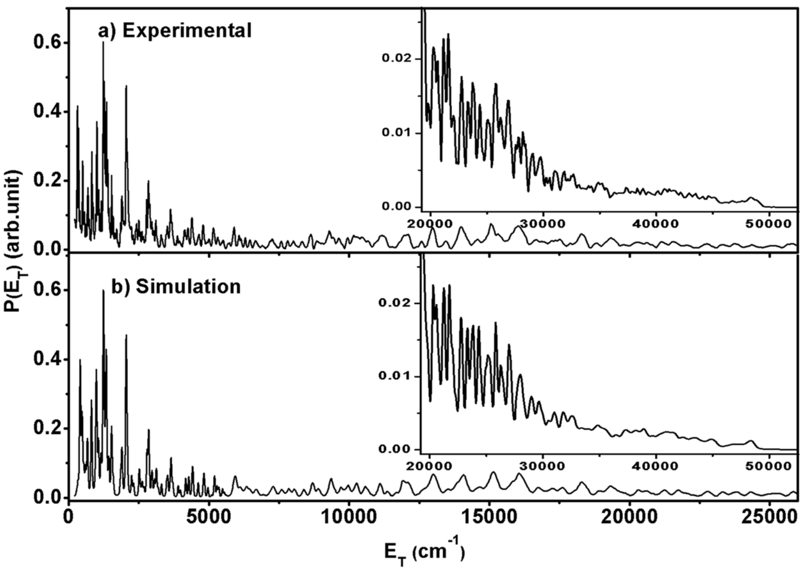

FIG. 2. The experimental (a) and simulated (b) product translational energy distributions for the photodissociation of H_2O at 111.5 nm with the detection axis parallel to photolysis laser polarization.

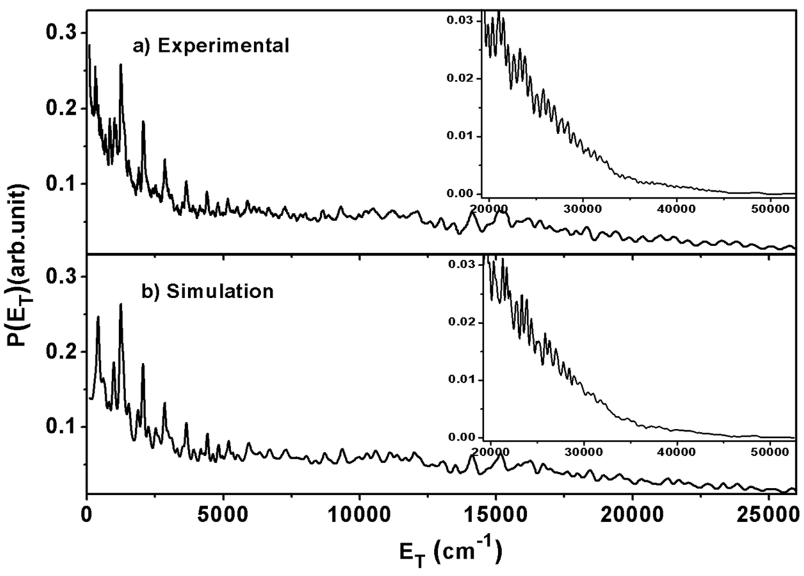

FIG. 3. The experimental (a) and simulated (b) product translational energy distributions for the photodissociation of H_2O at 111.5 nm with the detection axis perpendicular to photolysis laser polarization.

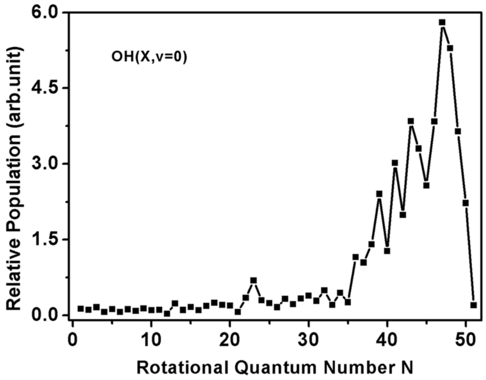

FIG. 4. The total rotational state distribution of the OH (X, $v = 0$) product from the photodissociation of H_2O at 111.5 nm.

(~75 V/cm) mounted across the intersection region. Since the 121.6 nm laser light also generates the photodissociation signals, a background subtraction scheme is performed by alternating the photolysis laser on and off. The neutral H atom products, after flying about 28 cm, are then field ionized and detected by a Z-stack microchannel plate (MCP) detector mounted on a rotational detector. Then the signal is amplified by a fast preamplifier and counted by a multichannel scaler.

III. EXPERIMENTAL RESULTS

A. Product translational energy distributions

The time of flight (TOF) spectra of the H atoms from H_2O photodissociation at 111.5 nm have been measured by using the above experimental methods. TOF spectra with the detection axis parallel (0°) and perpendicular (90°) to the photolysis laser polarization are both recorded. In addition, the TOF spectrum at the magic angle (~55°) is also recorded in order to make sure that the polarization direction is accurate. Figure 1 shows the TOF spectra for parallel and perpendicular directions. The two TOF spectra have been converted to the total translational energy distribution by using the following equation:

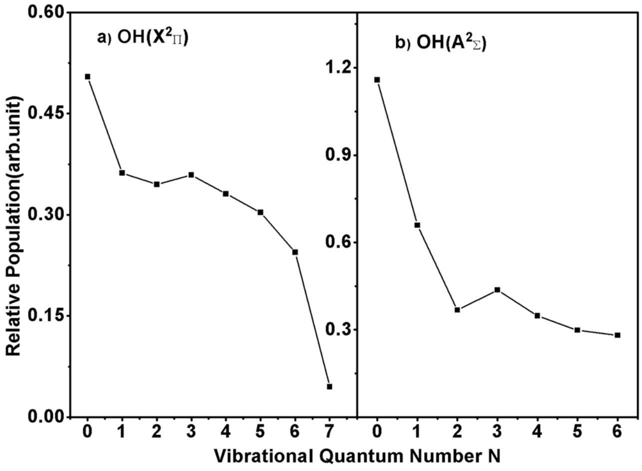

FIG. 6. Vibrational state distribution of the OH (X) product (a) and OH (A) product (b) from the photodissociation of H_2O at 111.5 nm.

$$E_T = \frac{1}{2}m_H\left(1 + \frac{m_H}{m_{OH}}\right)\left(\frac{d}{t}\right)^2, \tag{1}$$

where d is the flying path length of H atoms ($d \approx 28$ cm) and t is the measured time of flight. It is noted that the velocity of the molecular beam is also included in the conversion process. Figures 2(a) and 3(a) show the product translational energy distributions in the parallel and perpendicular directions, respectively. It is obvious that extensive sharp structures have been observed in the product translational energy distributions, which are similar to that observed in the H_2O photodissociation at lower (such as $\tilde{B}$) electronic excited states.[38]

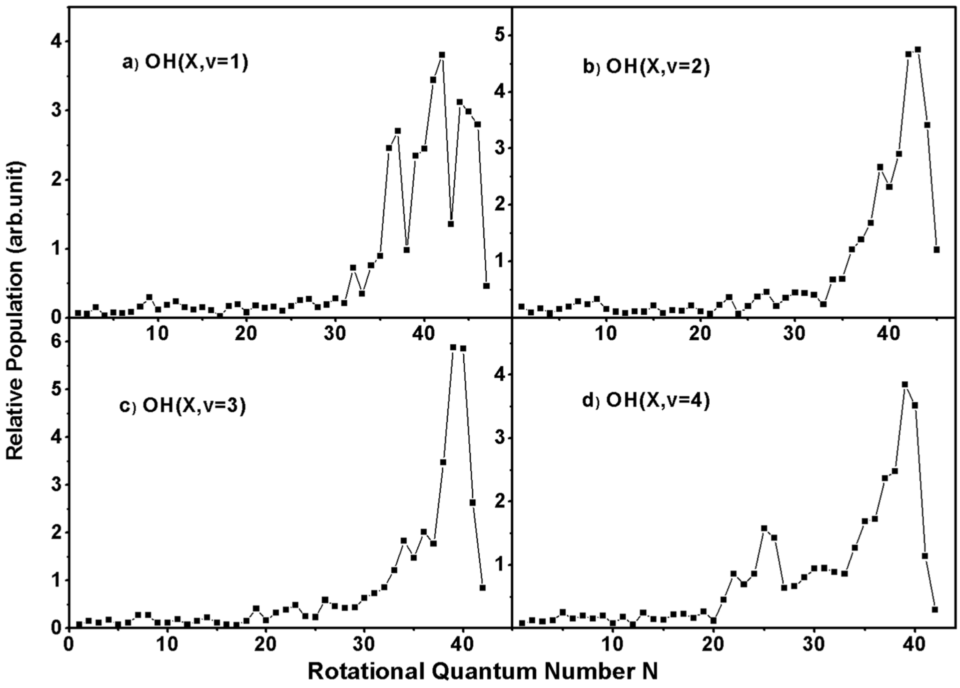

FIG. 5. Rotational state distributions of the OH (X, v = 1, 2, 3, 4) products from the photodissociation of H_2O at 111.5 nm.

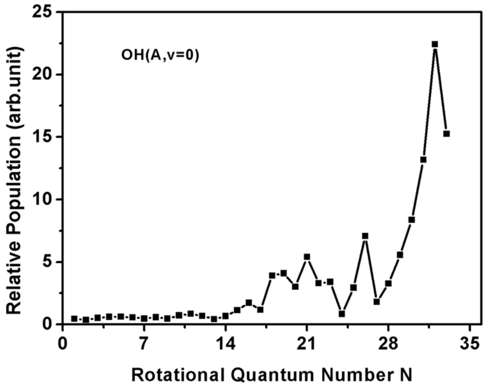

FIG. 7. The total rotational state distribution of the OH (A, v = 0) product from the photodissociation of H_2O at 111.5 nm.

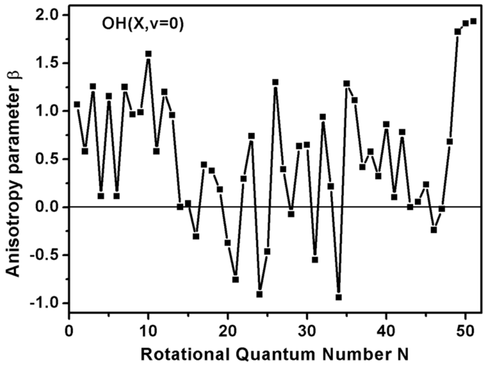

FIG. 9. Rotational dependence of the anisotropy parameter β for the OH (X, v = 0) product.

Since the H atom product has no internal excitation, these sharp features all correspond to the electronically and rovibrationally excited OH products. Based on the total energy conservation in the photolysis process, the group of structures located at the higher translational energy range corresponds to the ground electronic state OH (X) products, while the group of structures in the lower translational energy range corresponds to the electronically excited OH (A) products. It is noted that the structures belonging to OH (X) products are congested and partially resolved and are different from those observed in H_2O photodissociation at 121.6 nm,[38] suggesting high vibrational and rotational excitation of OH (X) products. In addition to the OH (X) and OH (A) products, a broad underlying energy distribution has also been observed with the peak locating at low translational energy, which can be assigned as the three-body dissociation O (^{3}P) + 2H channel.

In a one-photon molecular photodissociation process, the photodissociation product detected at an angle in the center-of-mass frame (θ_{cm}) relative to the photolysis light polarization can be represented by the following formula:

$$\Psi(\mathrm{E_T}, \theta_{\mathrm{cm}}) = \sigma(\mathrm{E_T})\{1 + \beta(\mathrm{E_T}) P_2(\cos\theta_{\mathrm{cm}})\}, \qquad (2)$$

where $\sigma(\mathrm{E_T})$ is the product translational energy distribution and $\beta(\mathrm{E_T})$ is the translational energy dependent anisotropy parameter. In this experiment, the translational energy distributions at two detections (parallel and perpendicular to photolysis laser polarization) are measured; therefore, $\beta(\mathrm{E_T})$ can be calculated.

B. Product quantum state distributions and anisotropy parameters

Assignments have been made for almost all the peaks in the translational energy spectra, and OH quantum state distributions can be determined from simulations of these translational energy spectra. The simulation method is the same with that described in Ref. 38. Figures 2(b) and 3(b) show the simulated product translational energy distributions for the two corresponding directions. The agreement between the experimental and simulated distributions is excellent. Figure 4

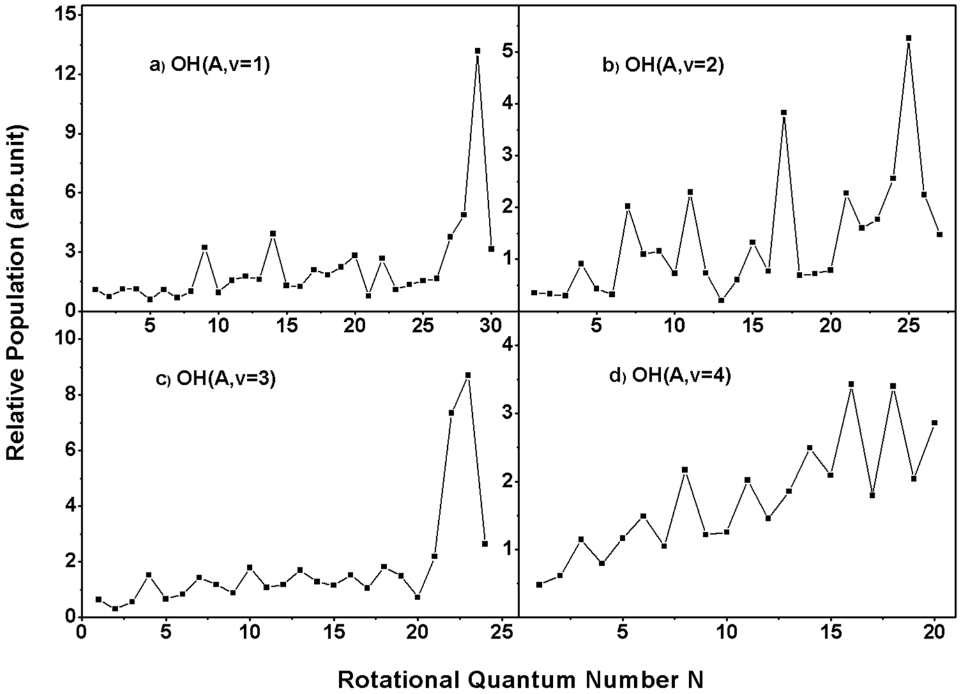

FIG. 8. Rotational state distributions of the OH (A, v = 1, 2, 3, 4) products from the photodissociation of H_2O at 111.5 nm.

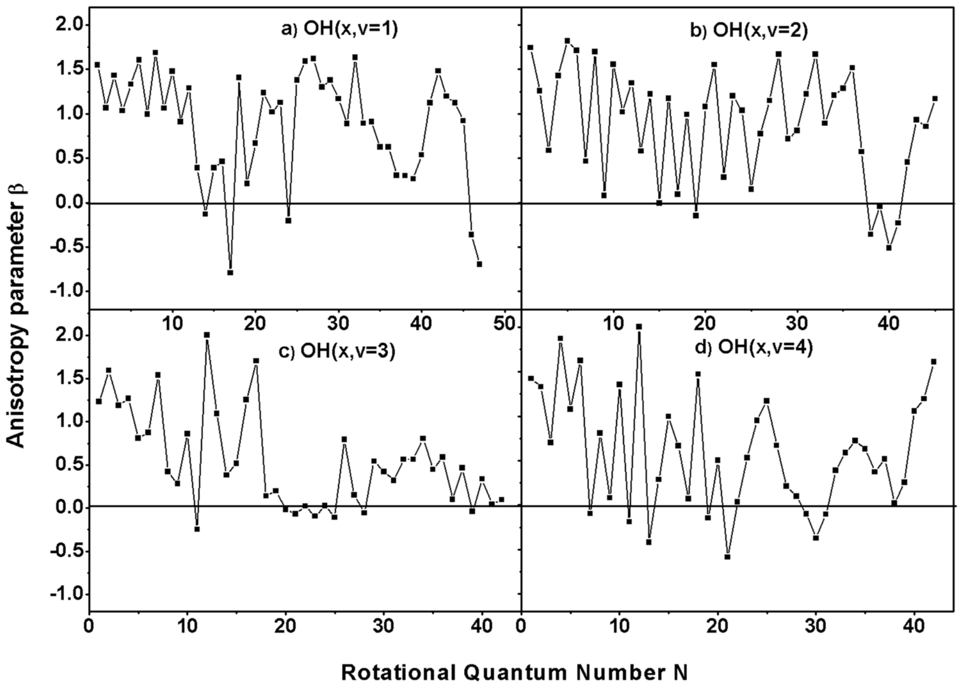

FIG. 10. Rotational dependence of the anisotropy parameter β for the OH (X, v = 1, 2, 3, 4) product.

shows the rotational distributions of the OH (X, v = 0) product obtained from the simulations. It is apparent that most of the OH (X, v = 0) products are extremely rotationally excited with a peak at N = 47, corresponding to about 33 400 cm^{-1} rotational energy, already 94% of the bond dissociation energy of the OH molecule. Such an extremely high rotational excitation has also been observed in the H_2O/HOD photodissociation at 121.6 nm, which is a direct consequence of strong forces at the conical intersections between the $\tilde{B}$- and the $\tilde{X}$-state surfaces for a linear H–O–H geometry.[35,38] It is noted that the rotational distribution obviously fluctuates as a function of rotational quantum number, which is similar to the previously observed population oscillations from dynamical interference through the two conical intersections between the $\tilde{B}$- and the $\tilde{X}$-state for the linear H–O–H and H–H–O geometries. However, the severe overlapping of the rotational manifolds for ground and excited vibrational levels prevent the direct observation of oscillations from the translational energy spectra. Figure 5 shows the rotational state distributions for the OH (X) products with v = 1-4. These products are also highly rotationally excited, with peaks at N = 41, 42, 39, 38, indicating that they are probably produced through the similar dynamical pathways as the OH (X, v = 0) product.

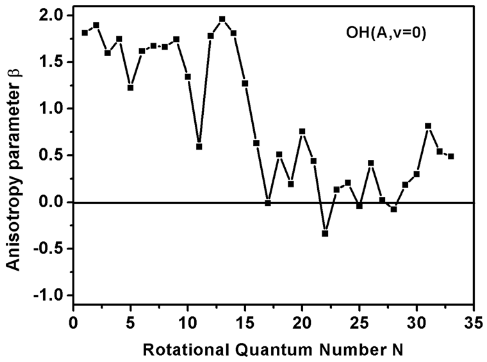

FIG. 11. Rotational dependence of the anisotropy parameter β for the OH (A, v = 0) product.

The vibrational distributions are obtained by integrating the rotational distribution for each vibrational level. Figure 6(a) shows the vibrational state distribution of the OH (X) products. Though the OH (X, v = 0) product is still the important channel, vibrationally excited OH products with v = 1-5 have modest population. The OH (X) product in the v = 0 level comprises only about 20% of the total OH (X) population, which is different from that observed in H_2O photodissociation at 121.6 nm, i.e., approximately half the total OH (X) population was observed.[38] This means the population of OH (X) product is strongly rotationally inverted but, in contrast to the previous results, is spread over a much wider range of vibrational excitation.

The OH product in the A electronic state has also been observed from the H_2O photodissociation at 111.5 nm. Figures 7 and 8 show the rotational state distributions of the OH (A) product for v = 0 and 1-4. For OH (A, v = 0 and 1) products, they are highly rotationally excited as in the ground state, with a peak at N = 32 and 29, close to the highest energetically accessible rotational levels, respectively. This indicates that the angular anisotropy of the potential is also very important for the dissociation of H_2O on the $\tilde{B}$ state surface since the OH (A) products adiabatically correlate with the $\tilde{B}$ state surface. The population of OH (A, v = 1-4) fluctuates strongly as a function of rotational quantum number yet has no regular pattern. Figure 6(b) shows the vibrational distribution for the OH (A) product. The OH (A, v = 0 and 1) products are dominant, while the populations of OH (A) with vibrational excitation of v = 2-6 are moderate. This is also different from that observed in H_2O photodissociation at 121.6 nm,[38] where the population of the OH (A) product decreases almost linearly as the vibrational energy increases.

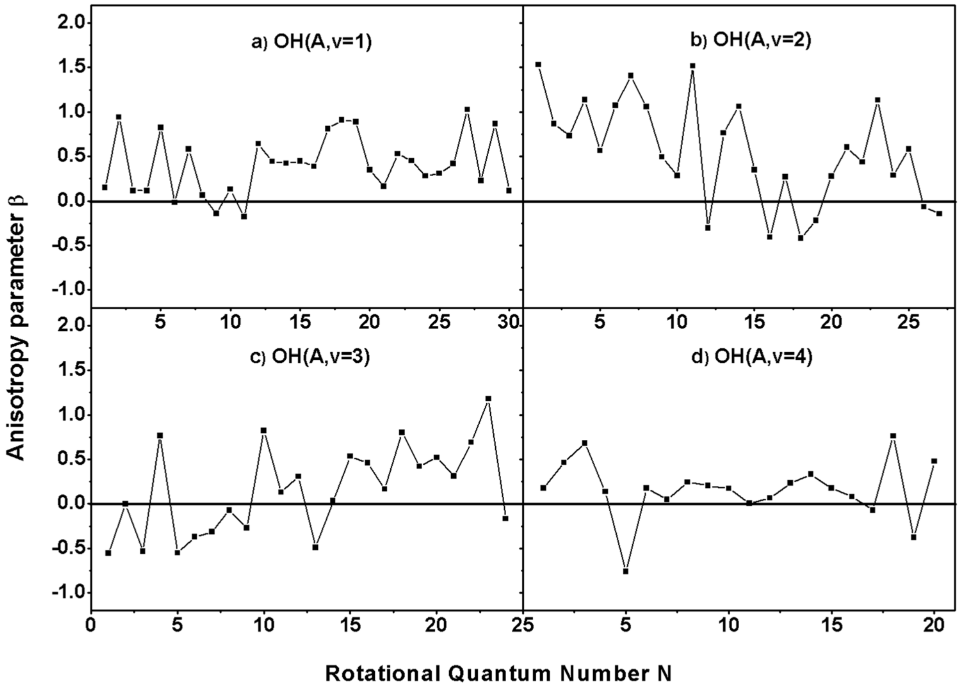

FIG. 12. Rotational dependence of the anisotropy parameter β for the OH (A, v = 1, 2, 3, 4) product.

From the OH product internal state distributions obtained in the parallel and perpendicular directions, the distributions of the angular anisotropy parameter for the various quantum levels of the OH product can be determined using Eq. (2). The $\beta(N)$ distribution for the OH (X) product in the $v = 0$ state is depicted in Fig. 9. It is apparent that a marked variation in the β parameter over the observed range of N values is displayed in this distribution spectrum. At lower rotational levels, the value of β fluctuates with N around 0.75, being moderately positive at N < 12, but varies widely as N increases. At higher rotational levels ($N > 34$), the β value turns positive again except for $N = 45$ and has a highest value at the highest rotational quantum number, 1.9 for $N = 49$. It is deduced from the varied β values that more than one mechanism is involved in the photodissociation process. Figure 10 shows the rotational distributions of the β parameters for OH (X) with v = 1-4. It is clear that the β parameters varied strongly as the N increases but are almost positive except for a small amount of rotational quantum number N. Obviously, these distributions are very different from that for the OH (X, $v = 0$) product, indicating the complex nature of H_2O photodissociation at 111.5 nm.

Anisotropy parameters have also been determined for the OH (A) product for v = 0–4. Figure 11 shows the rotational dependence of the β parameter for $v = 0$. At lower rotational levels ($N < 16$), the β value decreases from 1.8 to 0. At higher rotational level ($N > 17$), the value of the β parameter fluctuates around 0.25. The $\beta(N)$ distribution for the OH (A) product in the v = 1–4 state is shown in Fig. 12. Compared with OH (X, $v = 0$), the value of β for OH (A, v = 1–4) do not vary widely and keeps to be almost positive. For higher vibrational levels, such as OH (X, v = 5–7) and OH (A, v = 5–6), the β parameters cannot be determined accurately because of significant correlations via overlapping lines.

IV. DISCUSSIONS

We now seek to reveal the complicated VUV photodissociation dynamics. It is known that the molecular orbital configuration of water in the ground state is (core)^2...$(3a_1)^2(1b_1)^2$. Excitation of a $1b_1$ electron leads to Rydberg states converging to the ground state of the ion with bent geometry. The promotion of a $3a_1$ electron to a Rydberg orbital forms Rydberg series converging to the first excited state of the ion with quasilinear geometry. It is worth noting, however, that the vertical VUV Rydberg spectrum is largely dominated by bent to bent excitation (arising from the $nl \leftarrow 1b_1$ transition) and that very few observations of bent to linear (arising from the $nl \leftarrow 3a_1$ transition) have been reported.[15]

Many experimental and theoretical studies have focused on the $3d$ Rydberg states of water which exhibit very intense features in the absorption spectra. The rotationally resolved absorption spectra of $3d$ Rydberg states of water were first reported by Smith *et al.*[55] and then by Fillion *et al.*,[15] and three strong absorption bands were observed between 111 and 113 nm. These absorption bands have been assigned to four optically electronic transitions, namely, $\tilde{E}^1B_1$ ($3da_1 \leftarrow 1b_1$), $\tilde{E}'^1B_2$ ($3da_2 \leftarrow 1b_1$), and $\tilde{F}^1A_1$ ($3db_1 \leftarrow 1b_1$) degenerated with $\tilde{F}^1B_1$ ($3da_1' \leftarrow 1b_1$). In this work, the initial excitation of water at 111.5 nm is to $\tilde{F}^1A_1$ or $\tilde{F}^1B_1$ states. Excitation to the vibronic state $\tilde{E}(010)$ is also possible since the origin band of the $\tilde{E}(010)$ state is partially overlapped with the $\tilde{F}$ absorption band. Due to the relatively small transition probability from the ground state to the vibronic $\tilde{E}(010)$ state, the contribution from $\tilde{E}(010)$ state should be small. Though interesting dissociation dynamics are observed at this wavelength, the dissociation mechanism is not immediately clear since the potential energy surfaces of these Rydberg states of water are lacking. The observed rotational distributions and angular parameter distributions of OH (X) and OH (A) products are quite similar to those observed from water dissociation on the $\tilde{B}$ state, suggesting that there would be a predissociation pathway from the $\tilde{F}$ state to the $\tilde{B}$ state. *Ab initio* bending potential energy curves[14] showed that the $\tilde{F}$ state of water has the minima with a bond angle of about 110° which is comparable with the equilibrium bond angle of 108.9° for the molecular ion H_2O^+. For states of $^1A_1$ symmetry, complicated avoided crossings occur with the diabatic curves corresponding to the excitation $3db_1 \leftarrow 1b_1$ being crossed by those states arising from the excitations $3pa_1 \leftarrow 3a_1$ and $4s \leftarrow 3a_1$ for bond angles in the region of 135° and 145°, respectively.[14] Thus, the possible predissociation route would be a fast conversion from the initial excited $\tilde{F}^1A_1$ state to the higher-lying $^1A_1$ state ($3pa_1 \leftarrow 3a_1$) via an avoided crossing at the bent geometry, followed by a internal conversion to the $\tilde{D}^1A_1$ state ($3pa_2 \leftarrow 1b_1$), due to the near degeneracy of the $3p$ states ($^1A_1$ $3pa_1$ state and $\tilde{D}^1A_1$ $3pa_2$ state) at linear geometry with the bond length of around 1.8 bohrs.[56] Again, there is a well-known avoided crossing between the $\tilde{B}$ and $\tilde{D}$ states at the bond angle of about 100°; thus; the water molecule on the $\tilde{D}$ state has three possible pathways yielding H atoms: (1) fast internal conversion to the $\tilde{B}$ state and then direct dissociation on the $\tilde{B}$ state surface, yielding OH (A) and H products; (2) fast internal conversion to the $\tilde{B}$ state and then dissociation on the $\tilde{A}$ state via $\tilde{B}$-$\tilde{A}$ Renner-Teller coupling, but this pathway plays a minor role at a low rotational temperature of the parent molecules (~10 K[38]); (3) fast internal conversion to the $\tilde{B}$ state and then dissociation on the $\tilde{X}$ state via the $\tilde{B}$-$\tilde{X}$ conical intersections. Pathways (2) and (3) lead to OH (X) and H products. The branching ratios of the OH (A) and OH (X) products have been determined to be about 1.4:1 through the simulations, illustrating the relative importance of these different nonadiabatic dissociation pathways. The observed positive values of average anisotropy parameters for OH (X) and OH (A) products are consistent with the parallel transition $\tilde{F}^1A_1 \leftarrow \tilde{X}^1A_1$. For states of $^1B_1$ symmetry, the potential energy curves also have very complicated avoided crossings.[14] The initial excited $\tilde{F}^1B_1$ state can decay to the $\tilde{D}'^1B_1$ state via the $^1B_1$ $3pb_1$ state since there are avoided crossings between the $\tilde{F}^1B_1$ state and $^1B_1$ $3pb_1$ state at a bent angle of about 135° and between the $\tilde{D}'^1B_1$ state and $^1B_1$ $3pb_1$ state at a bent angle of about 165°. However, there is no obvious predissociation pathway from the $\tilde{D}'^1B_1$ state to the $\tilde{B}$ state, suggesting that the H atom products from the initial excited $\tilde{F}^1B_1$ state might be minor.

Though photodissociation dynamics of H_2O at 111.5 nm are similar with those at 121.6 nm, some differences still have been observed. The striking difference is the moderate vibrational excitation of OH (X) products at 111.5 nm compared with the cold vibrational excitation at 121.6 nm. *Ab initio* calculations by Harich *et al.*[38] showed that the extremely high rotational excitation of the OH product is mainly due to the dissociation through the conical intersection at the collinear (H–O–H) geometry between the $\tilde{B}$ and $\tilde{X}$ surfaces. The gradient of the $\tilde{B}$-state surface in the Franck-Condon region leads to the greatest initial acceleration in the bending coordinate towards collinear H–O–H, with lesser acceleration along the OH bonds, thus leaving a OH (X) radical with high angular momentum but little vibrational excitation. In addition, there is a second symmetry determined conical intersection on the $\tilde{B}$ state for the collinear O-H-H geometry. There is a barrier between the linear HOH and OHH region at $\gamma \approx 60°$. Thus, a small part of the dissociative flux on the $\tilde{B}$ state can pass through the second conical intersection if the photolysis energy is high enough to open this pathway. Harich *et al.*[38] pointed out that dissociation through this pathway leads to rotationally inverted OH (X) product with a much wider range of vibrational excitation due to the nature of surfaces at short H–H distances. At higher photolysis energy, the barrier at $\gamma \approx 60°$ has little effect. This suggests that more dissociative flux will pass through OHH conical intersection at 111.5 nm and lead to moderate vibrational excitation of OH (X) products. Further theoretical investigations are still needed for further understanding such complicated photodissociation dynamics.

V. CONCLUSIONS

In this work, we have performed an experimental study of the H_2O photodissociation on the $\tilde{F}$ state at 111.5 nm, by using the HRTOF technique combined with the VUV-FEL at DCLS. The translational energy distributions, as well as the state-resolved angular anisotropy parameters of the OH products, have been determined by measuring the H atom product TOF spectra. Experimental results show that OH (X) and OH (A) products are all highly rotationally excited and moderate vibrationally excited. Possible dissociation mechanisms are discussed. The present study would help us to understand the complicated dissociation process from the high Rydberg state of water molecules.

ACKNOWLEDGMENTS

K. J. Yuan acknowledges the support of the Strategic Priority Research Program of the Chinese Academy of Sciences (No. XDB17000000), the National Natural Science Foundation of China (No. 21673232), and Youth Innovation Promotion Association (No. 2014160). L. Che acknowledges the support of the National Natural Science Foundation of China (Nos. 21473015 and 21203016) and the Fundamental Research Funds for the Central Universities (No. 3132017067). C.Z.C. acknowledges the support of the National Natural Science Foundation of China (Nos. 21573227 and 21773236).

[1] P. B. Boncho, J. M. Michael, A. D. Michael, D. R. Neil, M.-S. Karen, S. E. Richard, and P. S. Daniel, Astrophys. J. **653**, 774 (2006).
[2] P. B. Boncho and J. M. Michael, Astrophys. J. **653**, 788 (2006).
[3] D. F. Plusquellic, O. Votava, and D. J. Nesbitt, J. Chem. Phys. **107**, 6123 (1997).
[4] R. D. Gilbert, M. S. Child, and J. W. C. Johns, Mol. Phys. **74**, 473 (1991).
[5] M. N. Ashfold, J. M. Bayley, R. N. Dixon, and J. D. Prince, Ber. Bunsengesellschaft Phys. Chem. **89**, 254 (1985).
[6] I. C. Lu, F. Wang, K. Yuan, Y. Cheng, and X. Yang, J. Chem. Phys. **128**, 066101 (2008).
[7] F. Xu, L. Wang, C. C. Martens, and Y. Zheng, J. Chem. Phys. **138**, 024103 (2013).
[8] Y. Cohen, I. Bar, and S. Rosenwaks, J. Chem. Phys. **102**, 3612 (1995).
[9] F. Stuhl and K. H. Welge, J. Chem. Phys. **47**, 332 (1967).
[10] M. N. R. Ashfold, J. M. Bayley, and R. N. Dixon, J. Chem. Phys. **79**, 4080 (1983).
[11] E. Segev and M. Shapiro, J. Chem. Phys. **77**, 5604 (1982).
[12] P. Andresen, G. S. Ondrey, B. Titze, and E. W. Rothe, J. Chem. Phys. **80**, 2548 (1984).
[13] K. Weide and R. Schinke, J. Chem. Phys. **87**, 4627 (1987).

[14] D. Hirst and M. Child, Mol. Phys. **77**, 463 (1992).

[15] J. H. Fillion, J. Ruiz, X. F. Yang, M. Castillejo, F. Rostas, and J. L. Lemaire, J. Chem. Phys. **120**, 6531 (2004).

[16] R. N. Dixon, T. A. Oliver, L. Cheng, Y. Cheng, K. Yuan, and X. Yang, J. Chem. Phys. **138**, 104306 (2013).

[17] S. Su, H. Wang, Z. Chen, S. Yu, D. Dai, K. Yuan, and X. Yang, J. Chem. Phys. **143**, 184302 (2015).

[18] L. Zhou, D. Xie, Z. Sun, and H. Guo, J. Chem. Phys. **140**, 024310 (2014).

[19] D. H. Mordaunt, M. N. R. Ashfold, and R. N. Dixon, J. Chem. Phys. **100**, 7360 (1994).

[20] A. Hodgson, J. P. Simons, M. N. Ashfold, J. M. Bayley, and R. N. Dixon, Ber. Bunsengesellschaft Phys. Chem. **89**, 251 (1985).

[21] A. Hodgson, J. P. Simons, M. N. R. Ashfold, J. M. Bayley, and R. N. Dixon, Mol. Phys. **54**, 351 (2006).

[22] R. G. Briggs, J. B. Halpern, G. Hancock, N. Shafizadeh, J. Rostas, J. L. Lemaire, and F. Rostas, Chem. Phys. Lett. **156**, 363 (1989).

[23] S. Bell, J. Mol. Spectrosc. **16**, 205 (1965).

[24] K. Weide, K. Kühl, and R. Schinke, J. Chem. Phys. **91**, 3999 (1989).

[25] H. t. Wang, W. S. Felps, and S. P. McGlynn, J. Chem. Phys. **67**, 2614 (1977).

[26] X. F. Yang, D. W. Hwang, J. J. Lin, and X. Ying, J. Chem. Phys. **113**, 10597 (2000).

[27] D. W. Hwang, X. Yang, and X. Yang, J. Chem. Phys. **110**, 4119 (1999).

[28] D. Häusler, P. Andresen, and R. Schinke, J. Chem. Phys. **87**, 3949 (1987).

[29] H. Guo and J. N. Murrell, Mol. Phys. **65**, 821 (1988).

[30] H. Guo and J. N. Murrell, J. Chem. Soc., Faraday Trans. 2 **84**, 949 (1988).

[31] Y. Wu and V. S. Batista, J. Phys. Chem. B **106**, 8271 (2002).

[32] R. N. Dixon, D. W. Hwang, X. F. Yang, S. Harich, J. J. Lin, and X. Yang, Science **285**, 1249 (1999).

[33] H. J. Krautwald, L. Schnider, K. H. Welge, and M. N. Ashfold, Faraday Discuss. Chem. Soc. **82**, 99 (1986).

[34] B. Heumann, K. Kühl, R. Düren, B. Hess, U. Meier, S. D. Peyerimhoff, and R. Schinke, Chem. Phys. Lett. **166**, 385 (1990).

[35] S. A. Harich, X. F. Yang, X. Yang, R. van Harrevelt, and M. C. van Hemert, Phys. Rev. Lett. **87**, 263001 (2001).

[36] S. A. Harich, X. Yang, D. W. H. Hwang, J. J. Lin, X. Yang, and R. N. Dixon, J. Chem. Phys. **114**, 7830 (2001).

[37] S. A. Harich, X. Yang, and R. N. Dixon, Phys. Rev. Lett. **87**, 253201 (2001).

[38] S. A. Harich, D. W. H. Hwang, X. Yang, J. J. Lin, X. Yang, and R. N. Dixon, J. Chem. Phys. **113**, 10073 (2000).

[39] D. W. Hwang, X. F. Yang, S. Harich, J. J. Lin, and X. Yang, J. Chem. Phys. **110**, 4123 (1999).

[40] A. Hodgson, J. P. Simons, M. N. Ashfold, J. M. Bayley, and R. N. Dixon, Chem. Phys. Lett. **107**, 1 (1984).

[41] M. N. R. Ashfold, J. M. Bayley, and R. N. Dixon, Can. J. Phys. **62**, 1806 (1984).

[42] H. H. Kuge and K. Kleinermanns, J. Chem. Phys. **90**, 46 (1989).

[43] M. N. R. Ashfold, J. M. Bayley, and R. N. Dixon, Chem. Phys. **84**, 35 (1984).

[44] C. H. Yang, G. Sarma, J. J. Ter Meulen, D. H. Parker, and C. M. Western, Phys. Chem. Chem. Phys. **12**, 13983 (2010).

[45] K. Yuan, Y. Cheng, L. Cheng, Q. Guo, D. Dai, X. Wang, X. Yang, and R. N. Dixon, Proc. Natl. Acad. Sci. U. S. A. **105**, 19148 (2008).

[46] K. Yuan, R. N. Dixon, and X. Yang, Acc. Chem. Res. **44**, 369 (2010).

[47] Z. He, D. Yang, Z. Chen, K. Yuan, D. Dai, G. Wu, and X. Yang, Phys. Chem. Chem. Phys. **19**, 29795 (2017).

[48] R. van Harrevelt and M. C. van Hemert, J. Chem. Phys. **112**, 5777 (2000).

[49] K. Yuan, L. Cheng, Y. Cheng, Q. Guo, D. Dai, and X. Yang, J. Chem. Phys. **131**, 074301 (2009).

[50] Y. Chang, S. Yu, H. Wang, S. Su, Z. Chen, L. Che, X. Wang, W. Zhang, D. Dai, G. Wu, K. Yuan, and X. Yang, "Tunable VUV photochemistry using vacuum ultraviolet free electron laser combined with H-atom Rydberg tagging time-of-flight spectroscopy," Rev. Sci. Instrum. (submitted).

[51] L.-H. Yu, M. Babzien, I. Ben-Zvi, L. F. DiMauro, A. Doyuran, W. Graves, E. Johnson, S. Krinsky, R. Malone, I. Pogorelsky, J. Skaritka, G. Rakowsky, L. Solomon, X. J. Wang, M. Woodl, V. Yakimenko, S. G. Biedron, J. N. Galayda, E. Gluskin, J. Jagger, V. Sajaev, and I. Vasserman, Science **289**, 932 (2000).

[52] L. Schnieder, W. Meier, K. H. Welge, M. N. R. Ashfold, and C. M. Western, J. Chem. Phys. **92**, 7027 (1990).

[53] K. Yuan, L. Cheng, Y. Cheng, Q. Guo, D. Dai, and X. Yang, Rev. Sci. Instrum. **79**, 124101 (2008).

[54] J. P. Marangos, N. Shen, H. Ma, M. H. R. Hutchinson, and J. P. Connerade, J. Opt. Soc. Am. B **7**, 1254 (1990).

[55] P. L. Smith, K. Yoshino, H. E. Griesinger, and J. H. Black, Astrophys. J. **250**, 166 (1981).

[56] I. D. Petsalakis, G. Theodorakopoulos, and M. S. Child, J. Phys. B: At., Mol. Opt. Phys. **28**, 5179 (1995).